iJRASET
International Journal For Research in Applied Science and Engineering Technology

INTERNATIONAL JOURNAL FOR RESEARCH

IN APPLIED SCIENCE & ENGINEERING TECHNOLOGY

Volume: 5 **Issue:** VIII **Month of publication:** August 2017

DOI: http://doi.org/10.22214/ijraset.2017.8263

www.ijraset.com

Call: 08813907089 | E-mail ID: ijraset@gmail.com

International Journal for Research in Applied Science & Engineering Technology (IJRASET)
ISSN: 2321-9653; IC Value: 45.98; SJ Impact Factor:6.887
Volume 5 Issue VIII, August 2017- Available at www.ijraset.com

Enhanced Photocatalytic Performance of ZnO Loaded Cotton Stalk Activated Carbon Composite on MB and RHB Dyes Under Sunlight Irradiation

P. Prabu[1], K. Raghu[2]
[1]*Department of Physics, Annamalai University, Annamalai Nagar, India*
[2]*Department of Physics, T.V.K. Govt. Arts College, Thiruvarur, India*

Abstract: ***Zinc oxide nanoparticles (ZnO) and ZnO loaded cotton stalk activated carbon (Zno/CSAC) were synthesized by chemical precipitation method and were used as photocatalyst for the degradation of two azo dyes (Methylene Blue and Rhodamine B) in aqueous solution under sunlight irradiation. The prepared samples were characterized by X-Ray diffraction (XRD), Fourier transform infrared (FT-IR) spectroscopy, UV-vis diffuse reflectance spectroscopy (DRS), Photoluminescence spectroscopy (PL) and Scanning electron microscopy (SEM) with energy dispersive X-ray analysis (EDX). The effects of key operation parameters such as amount of catalyst and contact time on the photodegradation of Methylene Blue and Rhodamine B were studied. ZnO/CSAC composites exhibited enhanced photocatalytic activity compared to pure ZnO particles. Pseudo-first order and pseudo-second order models were used to analyze the kinetics.***
Keywords: ZnO, ZnO/CSAC, Methylene Blue, Rhodamine B, Adsorption Kinetics

I. INTRODUCTION

Dyes are widely used in textile, rubber, paper, plastic and cosmetic industries. They discharge high amount of dyes into the water bodies every day [1] and nowadays, this has become one of the most serious environmental problems. Methylene blue (MB) is the cationic dye commonly used for coloring. It is generally used for dyeing cotton, wool, and silk. MB can cause eye burns and irritation to the skin in humans and animals and if ingested, can cause irritation to the gastrointestinal tract, nausea, vomiting, and diarrhea [2]. Rhodamine B is a basic dye widely used as a colorant in textiles and food materials and as biological stains in biochemical laboratories at high concentrations. It causes irritation to skin, eyes and respiratory tract if ingested by animals and human beings [3].

Photocatalysis, an advanced oxidation technology employing semiconductors as photocatalysts, is a promising method for treatment of contaminated ground, surface, and wastewater containing various organic pollutants [4–7]. Various semiconductors such as ZnO [8], CdS [9] and TiO_2 [10] have been used as photocatalysts. Among them, ZnO has become very well established in photocatalytic approaches as well as in the environmental catalysis area [11]. ZnO is a semiconductor with a wide band gap (3.3 eV), large exciton binding energy. It is abundant in nature and environment friendly. These characteristics make this material attractive for many applications such as solar cells, optical coatings, photocatalysts, antibacterial materials, electrical devices, active medium in UV semiconductor lasers and in gas sensors [12]. The photocatalytic activity of ZnO was recently recognized to be comparable with TiO_2 and has received much attention because of its high photosensitivity and stability in degrading various toxic substances [11].

The mechanism of photocatalytic reaction is based on the generation of electron–hole pairs. When a photocatalyst is illuminated, the photo-excited electron migrates from the valence band (VB) to the conduction band (CB) and holes are formed in valence band; these holes can generate hydroxyl radicals, which are highly reactive and oxidizing in nature [13].

Activated carbon (AC) is a nontoxic and low cost adsorbent used for the removal of pollutants such as dyes and heavy metals from the waste water due to its high surface area, porous structure, large adsorption capacity and fast adsorption kinetics [14,15]. Composites consisting of ZnO supported on activated carbon have shown remarkable results in inhibiting bacteria growth [16] and removing metals from aqueous solutions [17].

Present study reports the photocatalytic performance of ZnO nanoparticles supported on cotton stalk activated carbon towards degradation of Methylene blue and Rhodamine B under sunlight irradiation. Activated carbon was prepared from cotton stalk by chemical activation using phosphoric acid as activating agent. ZnO photocatalyst and ZnO loaded activated carbons (ZnO/CSACs) were synthesised by chemical precipitation and were characterized by XRD, FTIR spectroscopy, SEM with EDX, UV-DRS, PL and UV–Vis. spectroscopy. Photocatalytic degradation of dyes and adsorption kinetics of photocatalysis were studied.

II. MATERIALS AND METHODS

A. Materials

Phosphoric acid (H_3PO_4) and Sodium Hydroxide pellets (NaOH) were purchased from Merck, India. Zinc nitrate hexahydrate [$Zn(NO_3)_2.6H_2O$] and Rhodamine B were purchased from SD fine chemicals Mumbai and Methylene blue from Loba chemicals, India. All are chemicals are of analytical reagent grade and were used without further purification. Distilled water was used throughout the experiments.

Cotton Stalk (CS) was collected from local agriculture area in Tranquebar taluk in Nagapattinam district, Tamilnadu, India. It was washed several times to remove the impurities and then dried in hot air oven at 110˚ C for 24 h. The dried material was then ground and sieved to obtain precursors of particle sizes less than 2 mm.

B. Preparation of Cotton Stalk Activated Carbon (CSAC)

The powdered cotton stalk was impregnated in phosphoric acid solution in the ratio of 1:2 (weight of precursor: volume of H_3PO_4) and the mixture was stirred continuously using a magnetic stirrer at ambient temperature for 5 h. The precursor was kept soaked for 24 h followed by filtering and drying in hot air oven at 110˚C for 24 h. The dried mixture was then heated at the rate of 20˚C min^{-1} to and kept at 600˚C for 2 h in a muffle furnace and then cooled down to room temperature. The materials were then washed sequentially with 0.1M NaOH solution, hot distilled water and finally with cold distilled water to remove residual acids until the washing solution become neutral. The washed sample was dried in hot air oven at 110˚C for 6h and cooled to room temperature to obtain the cotton stalk activated carbon.

C. Preparation of ZnO and ZnO/CSAC

0.5 M [$Zn(NO_3)_2 \cdot 6H_2O$] was dissolved in 100 mL distilled water to prepare zinc nitrate solution and 1.0 M (NaOH) was dissolved in 100 mL distilled water to prepare sodium hydroxide solution. NaOH solution was added drop wise to the vigorously stirred zinc nitrate solution at 70° C for about 5 h, until a white precipitate is formed. After cooling to room temperature the precipitate was filtered using Whatman filter paper (11mm) and washed several times with distilled water and ethanol. The precipitate was then dried in hot air oven at 100° C for 3 h and then ground into a powder using an agate mortar. Finally the powder was calcined at 500 °C for 2 h at a heating rate of about 20 ° C per minute in a muffle furnace to obtain ZnO. The composite catalysts (ZnO/CSACs) were prepared by the same method but by adding 20, 40 and 60 wt. % of cotton stalk activated carbon in zinc nitrate solution and were named as ZnO/CSAC-20, ZnO/CSAC-40 and ZnO/CSAC-60 respectively.

D. Characterization of ZnO and ZnO/CSACs

XRD patterns were obtained using an XPERT-PRO Gonio scan-2 with a graphite monochromator equipped with Cu Kα as radiation source (λ= 1.5406 Å) at 40 kV/30 mA. The surface functional groups were analysed from FT-IR spectra obtained by the KBr pellet method using Perkin Elmer Spectrum RXI FTIR spectrometer in the range 4000–400 cm^{-1}. The morphology and chemical composition of the catalysts were investigated by using SEM (VEGA3 TESCAN) equipped with energy dispersive X-ray spectrometer (Bruker). The band gap energy was determined using UV-DRS spectra recorded using a Shimadzu UV-3600 plus UV-VIS-NIR spectrophotometer. To determine the optical and photochemical properties of catalysts, room temperature PL spectra were recorded using a Perkin-Elmer LS 55 fluorescence spectrometer. Photocatalytic degradation process was monitored using Shimadzu UV-1800 spectrophotometer by measuring absorbance of the dye solution at λ_{max} of MB at 664 nm and RhB at 554 nm.

E. Adsorption and Photocatalytic Experiments

All photocatalytic degradation experiments were carried out under similar sunny conditions on days between 11am and 2pm in the month of April-May 2016. Solar intensity (1250 × 100± 100 lx) was almost constant during the experiments. To 100 mL of aqueous dye solutions (30 mg/L) taken separately in 250mL vessels, an appropriate quantity of ZnO or ZnO/CSAC (0.40 g/L) was added and the contents were magnetically stirred at 550 rpm under direct sunlight. The higher dosage of catalyst may not be useful since aggregation may reduce the irradiation field due to light scattering **[**18**]**. At different time intervals, about 5 mL of suspension was sampled and absorption (at 664 nm for MB and 554 nm for RhB) was analysed using UV–vis spectrophotometer. The percentage degradation of dyes was calculated using the following equation.

$$\% \text{ Degradation} = \frac{C_o - C_t}{C_o} \times 100 \qquad (1)$$

The amount of dye adsorbed at time t, q_t (mg/g), was calculated by the following equation.

$$q_t = \frac{(C_o - C_t)V}{m} \qquad (2)$$

where, C_o is the initial concentration of dye solution (mg/L), C_t is the concentration of dye after irradiation at specific time interval (mg/L), V (mL) is the volume of solution, and m (g) is the mass of catalyst used.

III. RESULTS AND DISCUSSION

A. XRD Analysis

The X-ray diffraction patterns of CSAC, ZnO, and ZnO/CSACs are shown in Fig.1. The pattern for CSAC (Fig. 1a) shows no sharp peaks but two broad humps at about $2\theta \approx 25^\circ$ and 43° corresponding to (002) and (100) planes of the carbon structure, revealing a predominantly amorphous structure. The ZnO shows a series of peaks observed at 2θ = 31.72˚, 34.38˚, 36.21˚, 47.50˚, 56.55˚, 62.80˚, 66.33˚, 67.88˚, 69.01˚, 72.58˚ and 76.98˚ corresponding to the (100), (002), (101), (102), (110), (103), (200), (112), (201), (004) and (202) planes of the hexagonal ZnO structure, respectively. All these peaks are in good agreement with the standard diffraction pattern of wurtzite (hexagonal) structure of ZnO (JCPDS-79-2205). There are no additional peaks corresponding to any impurities or hydroxides indicating the purity of ZnO nanoparticles. All ZnO/CSACs exhibited similar patterns revealing no change in Zno structure upon loading on CSAC.

The average crystallite size of ZnO, and ZnO/CSACs were determined using the Debye-Scherrer's formula [19],

$$D = \frac{0.9\lambda}{\beta \cos\theta} \qquad (3)$$

Where D is the average crystallite size (nm), λ is the wavelength of X-rays (1.5406 Å), β is the full width at half maximum and θ is the Bragg's angle

The average crystallite size for ZnO was determined to be 35.15 nm. Upon increasing CSAC wt.%, the size was found to decrease from 34.07 nm for 20 wt.% to 32.45 nm for 40 wt.% and 28.36 nm for 60 wt.%. Thus ZnO/CSAC-60 with smaller crystallites has more surface area to enhance the adsorption.

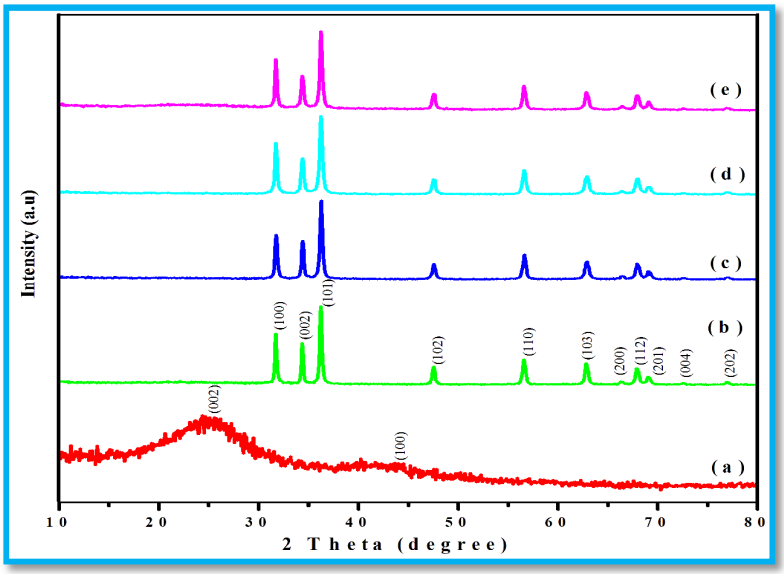

Fig.1. XRD patterns of (a) CSAC, (b) ZnO, (c) ZnO/CSAC-20, (d) ZnO/CSAC-40 and (e) ZnO/CSAC-60

B. FT-IR Analysis

FTIR spectra of CSAC, ZnO and ZnO/CSACs (20-60 wt. %) are shown in Fig.2. In CSAC, the wide band in the range of 3804–3200 cm^{-1} corresponds to the presence of O-H stretching vibration in hydroxyl groups [20]. The band at 1705 cm^{-1} is attributed to the stretching vibration of C=O in ketones, aldehydes, lactones, and carboxyl groups [21] and the band at about 1570 cm^{-1} is assigned to C=C vibration in aromatic rings [22]. These bands reflect the biological origin of the precursor. A shoulder at 1080 cm^{-1}

may represent the stretching vibrations of P-O-P arising from phosphorous containing carbonaceous structures owing to phosphoric acid activation [23]. The band at 497cm^{-1} is ascribed to deformation mode of P-O units.

In the FTIR spectra of ZnO and ZnO/CSACs (20-60 wt. %), Fig.2b and 2 c-e, the absorption peak at 3452 cm^{-1} corresponds to the O-H stretching of the surface adsorbed water molecule [24]. A highly intense absorption band in the range 610–400 cm^{-1} for pure ZnO and ZnO/CSACs (20-60 wt. %) corresponds to the deformation of Zn−O bond [25]. As CSAC wt. % increases, ZnO/CSACs exhibit gradual increase in the intensity of bands due C=O and P-O units in addition to the strong band due to Zn-O units.

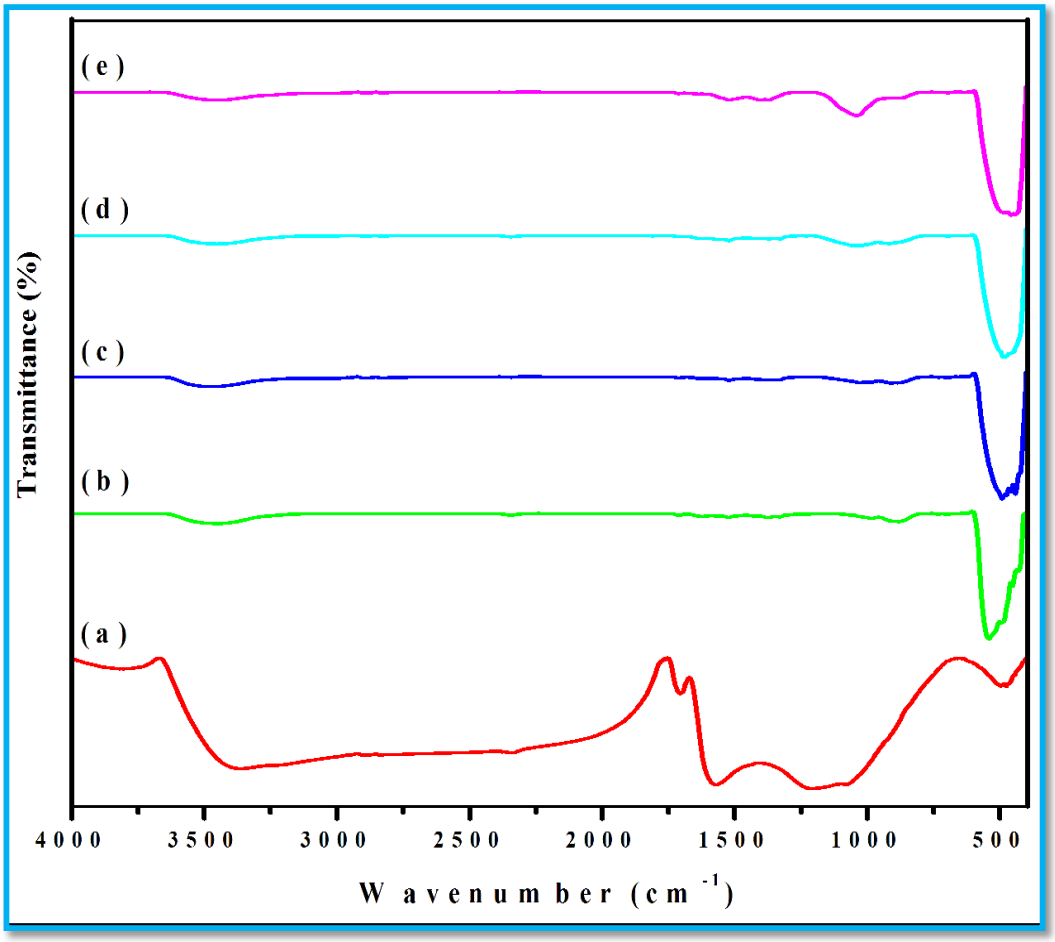

Fig.2. FT-IR spectra of (a) CSAC, (b) ZnO, (c) ZnO/CSAC-20, (d) ZnO/CSAC-40 and (e) ZnO/CSAC-60

C. UV-DRS Analysis

The diffuse reflectance spectra of ZnO and ZnO/CSACs recorded at 200-800 nm are depicted in Fig.3. The band gap energy (E_g) of the samples was measured by the wavelength values corresponding to the intersection point of the vertical and horizontal parts of the spectra, using the equation [26].

$$E_g = \frac{hc}{\lambda} eV \qquad (4)$$

where E_g is the band gap energy (eV), h is the Planck's constant, c is the light velocity and λ is the wavelength (nm). The band gap value of ZnO was found to be 3.35eV and that of ZnO/CSAC 20 wt.%, 40 wt.% and 60 wt.% to be 3.34eV, 3.33eV and 3.32eV respectively. Lower the band gap, higher will be the number of electron hole pair with ZnO/CSACs, to enhance the photocatalytic dye degradation.

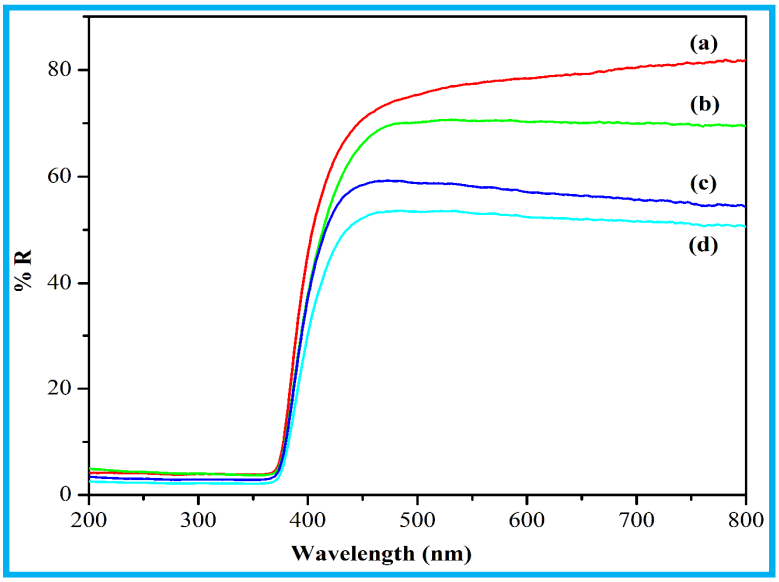

Fig.3. UV-Vis diffuse reflectance spectra (a) ZnO, (b) ZnO/CSAC-20, (c) ZnO/CSAC-40 and (d) ZnO/CSAC-60

D. *Photoluminescence (PL) Analysis*

Room-temperature PL spectra obtained with excitation wavelength of 325 nm for ZnO and ZnO/CSACs are shown in Fig. 4 (a-d). All the nanocomposites were characterised by four bands. The blue bands at around 420 and 482 nm correspond to band edge free excitons and bound excitons respectively [27], while the another blue emission present at around 458 nm is generally belived to arise from surface defects [28] . A number of hypotheses have been proposed to explain the green emission at 528 nm such as transition between electron close to the conduction band and a deeply trapped hole at V_o^{++}, surface defects like Zn^{2+} vacancies, due to the transition between *antisite* oxygen and donor-acceptor complexes, [29] and so on. Among ZnO/CSACs, there is no significant shift in the emission bands, with increasing CSAC content, the PL emission intensity has decreased. The lowest PL intensity in CSAC-ZnO-60, implies that the recombination of charge carriers is effectively suppressed by CSAC leading to a higher photocatalytic activity.

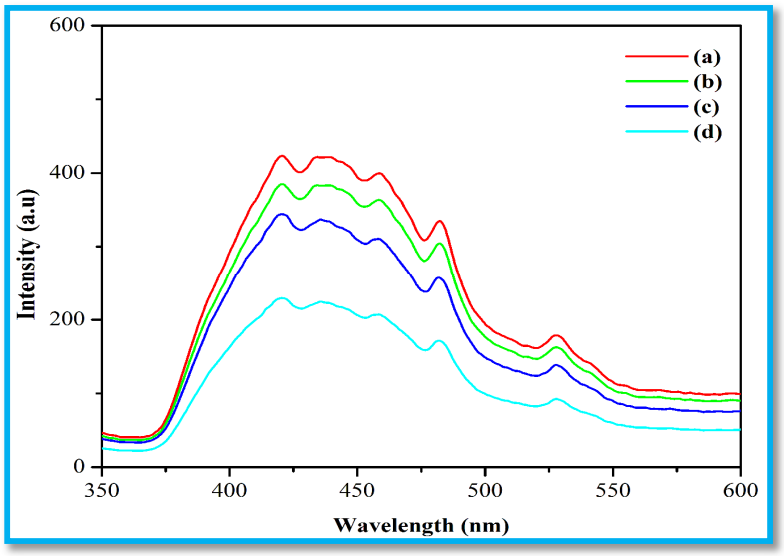

Fig.4. Room temperature PL spectra of (a) ZnO, (b) ZnO/CSAC-20, (c) ZnO/CSAC-40 and (d) ZnO/CSAC-60 with excitation wavelength (λ_{ex}) of 325 nm

E. Scanning Electron Microscopy (SEM) with EDX Analysis

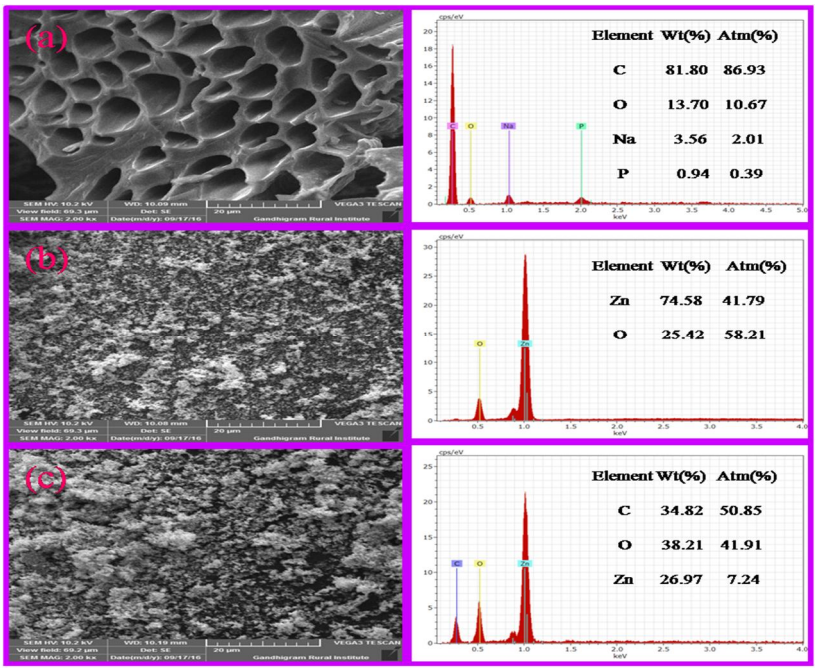

Fig.5. SEM-EDX images of (a) CSAC, (b) ZnO and (c) ZnO/CSAC-60

The SEM images of CSAC, ZnO and ZnO/CSAC-60 are shown in Fig. 5a-c along with their EDX analyses. CSAC exhibited highly porous honeycomb structure. ZnO exhibited a porous spongy network. ZnO/CSAC-60 revealed a homogeneous coverage of ZnO particles over activated carbon. The corresponding EDX patterns exhibited peaks for the relevant elemental composition indicating the purity of samples free of contamination.

F. Photocatalytic Performance of ZnO and ZnO/CSAC-60

1) *Effect of Catalyst Dosage:* The effect of ZnO and ZnO/CSAC-60 dosage on degradation of MB and RhB dye solutions under sunlight for 110 min is shown in Figs. 6a and 6b respectively. With both ZnO and ZnO/CSAC-60, the percent removal of dyes has increased on increasing catalyst dosage up to 0.40 g/L and above which the efficiency decreased. The early increase in removal efficiency can be attributed to increasing number of active adsorption sites as catalyst dosage increases. However, excess catalyst causes greater turbidity of the medium. Scattering of light by excess suspended moities reduces light penetration and ability to reach active sites and inhibit photodecolorization [30]. The optimum catalyst dosage was hence chosen as 0.40 g/L.

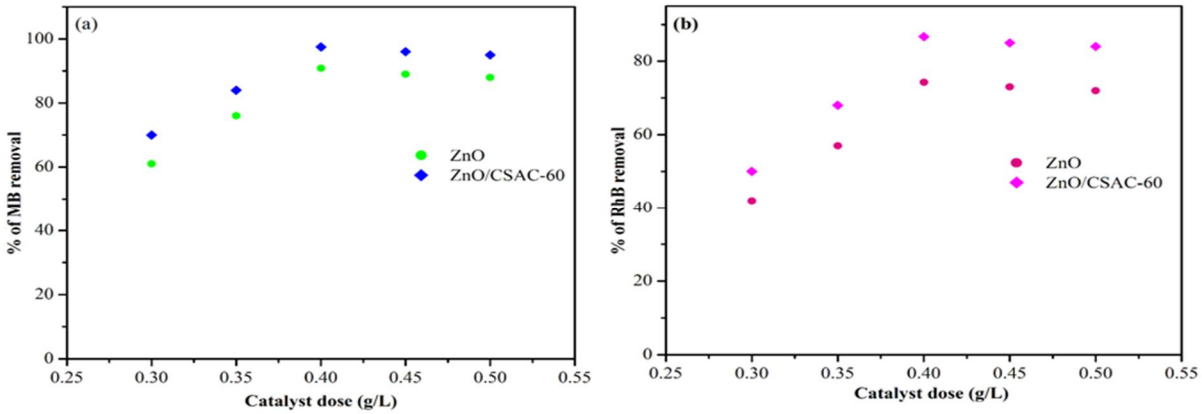

Fig.6. Effect of ZnO and ZnO/CSAC-60 dosage on photocatalytic degradation of (a) MB and (B) RhB

2) *Effect of Contact Time:* Contact time experiments were run with optimum ZnO and ZnO/CSAC-60 dosage (0.40 g/L) in 30 mg/L dye solutions for 110 min under sunlight irradiation. The photocatalytic activity of catalysts was evaluated in terms of percentage of dye degradation using Eq. (1) from the UV-Vis. Spectra recorded at different intervals (Fig. 7a and 7b.) and the results are depicted in Fig.8. The photo degradation efficiency of ZnO reached 90.87 % in MB and 74.27 % in RhB, after 110 min irradiation time. In case of ZnO/CSAC-60, the removal efficiency of MB reached 97.52 % and that of RhB reached 86.67% after the same irradiation time.

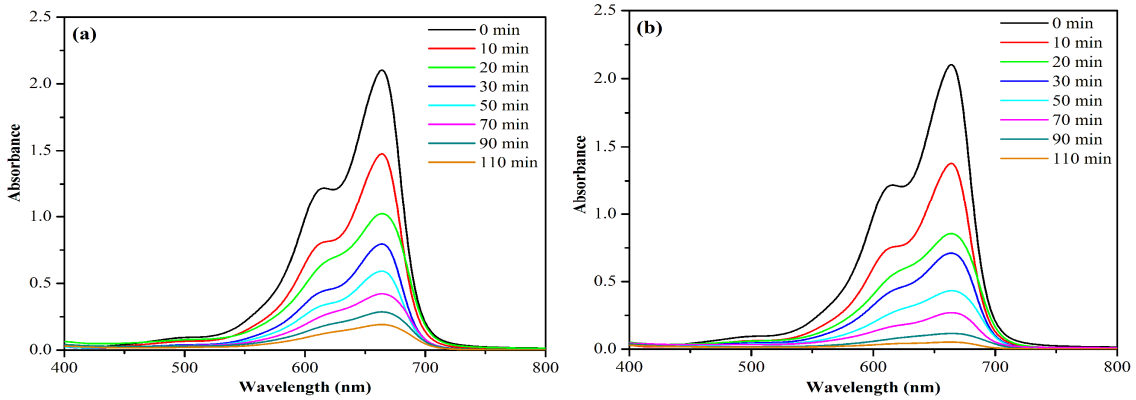

Fig.7a. UV-Vis absorption spectra of MB in presence of (a) ZnO and (b) ZnO/CSAC-60 at different time intervals

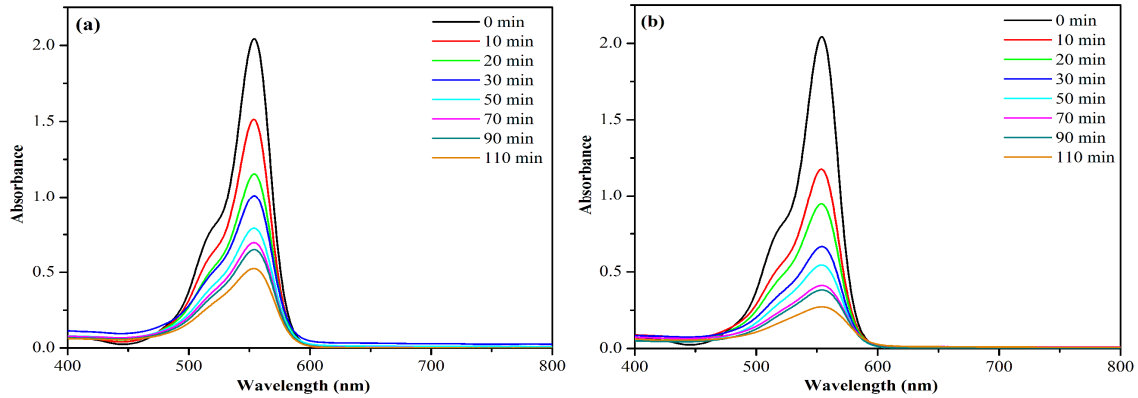

Fig.7b. UV-Vis absorption spectra of RhB in presence of (a) ZnO and (b) ZnO/CSAC-60 at different time intervals

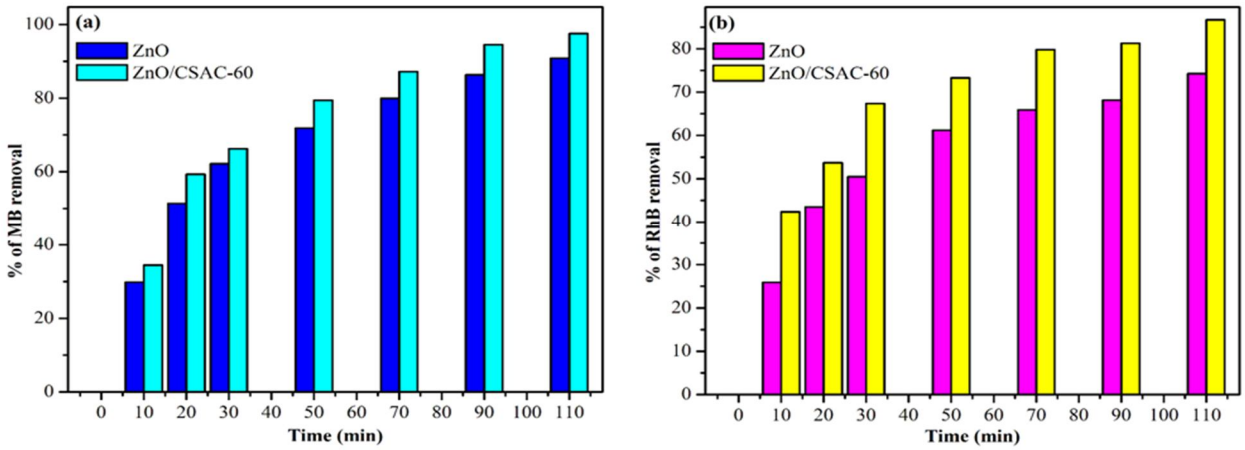

Fig.8. Effect of contact time on Photocatalytic degradation of (a) MB and (b) RhB in presence of ZnO and ZnO/CSAC-60

3) *Adsorption Kinetics:* The kinetics of photocatalytic degradation of MB and RhB by ZnO and Zno/CSAC-60 was studied by measuring percent removal of dyes using UV-Visible spectroscopy. Pseudo-first-order and pseudo-second-order models were applied to fit the experimental data to analyze the adsorption kinetics.

4) *Pseudo-First Order Model:* The Pseudo-first order model [31] is expressed as:

$$\log(q_e - q_t) = \log q_e - \frac{k_1}{2.303} t \qquad (5)$$

where q_e (mg /g) and q_t (mg /g) are the amount of dye adsorbed on sorbent at equilibrium and time t, respectively. k_1 (min^{-1}) is the pseudo-first order rate constant. The values of k_1 and q_e, can obtained from the slope and intercept of plot of log (q_e-q_t) versus time t (Fig.9a and 9b), and the values are presented in Table.1

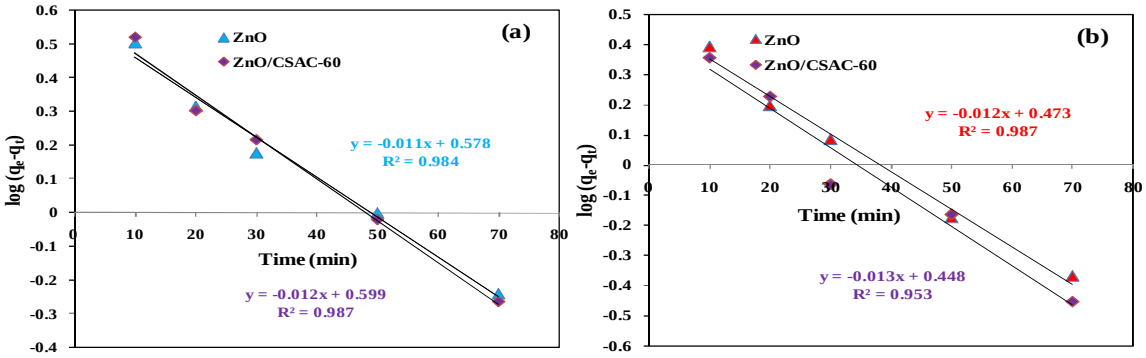

Fig.9. Pseudo-first-order model for the adsorption of (a) MB and (b) RhB onto ZnO and ZnO/CSAC-60 (Catalyst dose = 0.40 g/L)

5) *Pseudo-Second Order Model:* The Pseudo-second order model [32] is expressed as:

$$\frac{t}{q_t} = \frac{1}{k_2 q_e^2} + \frac{t}{q_e} \qquad (6)$$

where q_e is the amount of adsorbate adsorbed per unit mass of sorbent at equilibrium (mg/g), q_t is the amount of adsorbate adsorbed at contact time t (mg/g) and k_2 is Pseudo-second order constant (g/mg min^{-1}). The values of k_2 and q_e were calculated from the slope and intercept of plots of t/q_t versus time t (Fig.10a and 10b). The initial adsorption rate denoted as h (mg/g min^{-1}) is given as:

$$h = k_2 q_e^2 \qquad (7)$$

The calculated values of k_2, q_e and h are presented in Table1. Compared to pseudo-first-order model, pseudo-second order model exhibited higher value of correlation coefficients R^2 and also calculated q_e values are more closer to experimental values. This implies that the adsorption is better explained by pseudo-second-order kinetic model rather than pseudo-first-order. Because, the pseudo-first-order and pseudo-second-order interactions were based on physisorption and chemisorption processes [33], respectively, the adsorption of both dyes onto catalyst in the present case may be chemisorption process.

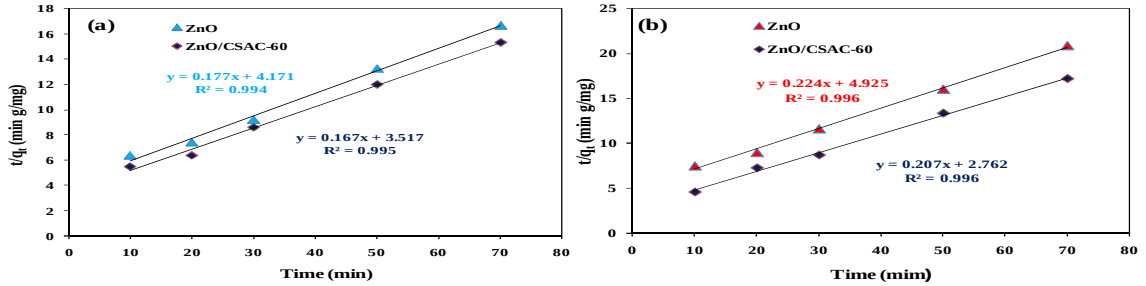

Fig.10. Pseudo-second-order model for the adsorption of (a) MB and (b) RhB onto ZnO and ZnO/CSAC-60 (Catalyst dose = 0.4 g/L)

Table.1. Kinetics parameters for pseudo-first-order and pseudo-second-order models for the adsorption of MB and RhB onto ZnO and ZnO/CSAC-60

C_o (mg/L)	catalyst	q_e, exp (mg/g)	Pseudo-first order model			Pseudo-second order model			
			K_1 (min^{-1})	q_e, cal (mg/g)	R^2	K_2(g/mg min)	q_e,cal (mg/g)	h (mg/gmin)	R^2
30 MB	ZnO	4.7775	0.0253	3.7844	0.984	0.0750	5.6497	0.2397	0.994
	ZnO/CSAC-60	5.1275	0.0276	3.9719	0.987	0.0792	5.9880	0.2843	0.995
30 RhB	ZnO	3.79	0.0276	2.9716	0.987	0.0101	4.4642	0.2030	0.996
	ZnO/CSAC-60	4.4225	0.0299	2.8054	0.953	0.0155	4.8309	0.3620	0.996

IV. CONCLUSIONS

ZnO and ZnO/CSACs were synthesized by chemical precipitation method and were characterized by XRD, SEM with EDX, UV-DRS, PL and UV-Vis. spectrocopy. ZnO/CSACs exhibited homogeneous coverage of smaller crystallites exposing greater surface are for enhanced adsorption. They have registered lower band gap and PL emission intensity compared to bare ZnO, to enhance photocatalytic activity. ZnO/CSAC-60 has exhibited highest removal efficiency over MB and RhB in the present study. The kinetics of adsorption was better explained by pseudo-second order reaction revealing that the adsorption of dyes to be chemisorption process. ZnO/CSAC-60 with highest dye removal efficiency can be utilized as low cost adsorbent for removal of dyes.

REFERENCES

[1] T. Robinson, G. McMullan, R. Marchant, P. Nigam , Remediation of dyes in textile effluent: a critical review on current treatment technologies with a proposed alternative, Biores. Technol. 77 (2001) 247–255.
[2] S. Senthilkumaar , P.R. Varadarajan, K. Porkodi, C.V. Subbhuraam, Adsorption of methylene blue onto jute fiber carbon: kinetics and equilibrium studies, J. Colloid Interface Sci. 284 (2005) 78–82.
[3] R. Jaina, M. Mathura, S. Sikarwara, A. Mittal, Removal of the hazardous dye rhodamine B through photocatalytic and adsorption treatments, J. Environ. Manage. 85 (2007) 956–964.
[4] P.R. Gogate, A.B. Pandit, A review of imperative technologies for wastewater treatment I: oxidation technologies at ambient conditions, Adv Environ Res 8: (2004) 501-551.
[5] K. Kabra, R. Chaudhary, R.L. Sawhney, Treatment of Hazardous Organic and Inorganic Compounds through Aqueous-Phase Photocatalysis: A Review, Ind Eng Chem Res 43: (2004) 7683-7696.
[6] M.P. Reddy, A. Venugopal, M. Subrahmanyam, Hydroxyapatite photocatalytic degradation of calmagite (an azo dye) in aqueous suspension, Appl Catal B Environ 69: (2007) 164-170.
[7] O.K. Dalrymple, D.H. Yeh, M.A. Trotz, Removing pharmaceuticals and endocrine-disrupting compounds from wastewater by photocatalysis, J Chem Technol Biotechnol 82: (2007) 121-134.
[8] Y.H. Jang, S.T. Kochuveedu, M. Cha, Y.J Jang, J.Y. Lee, J. Lee, J. Lee, J. Kim, D.Y. Ryu, D.H. Kim, Synthesis and photocatalytic properties of hierarchical metal nanoparticles/ZnO thin films hetero-nanostructures assisted by diblock copolymer inverse micellar nanotemplates, Journal of Colloid and Interface Science 345 (2010) 125–130.
[9] T. Torimoto, H. Yoneyama, Photocatalytic reduction of CO, using surface-modified CdS photocatalysts in organic solvents, Journal of Photochemistry and Photobiology A, 113 (1998) 93–97.
[10] Y. Chen, E. Stathatos, D. Dionysiou, Microstructure characterization and photocatalytic activity of mesoporous TiO_2 films with ultrafine anatase nanocrystallites, Surface and Coatings Technology 202 (2008) 1944–1950.
[11] R. Saravanan, V.K. Gupta, V. Narayanan, A. Stephen, Comparative study on photocatalytic activity of ZnO prepared by different methods, J. Mol. Liq. 181 (2013)133–141.
[12] K. Sato, H. Katayama – Yoshida, Material design for transparent ferromagnets with ZnO-based magnetic semiconductors, Japanese Journal of Applied Physics 39 (2000) L555-L558.
[13] N. Elamin, A. Elsanousi, Synthesis of ZnO nanostructures and their photocatalytic activity. J Appl Ind Sci 1(1): (2013) 32–35.
[14] M. Ghaedi, H. Tavallali, M. Sharifi, S. Nasiri Kokhdan, A. Asghari, Preparation of low cost activated carbon from Myrtus communis and pomegranate and their efficient application for removal of Congo red from aqueous solution, Spectrochim. Acta, Part A 86 (2012) 107–114.
[15] F. Taghizadeh, M. Ghaedi, K. Kamali, E. Sharifpour, R. Sahraie, M.K. Purkait, Comparison of nickel and/or zinc selenide nanoparticle loaded on activated carbon as efficient adsorbents for kinetic and equilibrium study of removal of Arsenazo (III) dye, Powder Technol. 245 (2013) 217–226.
[16] O. Yamamoto, K. Nakakoshi, T. Sasamoto, H. Nakagawa, K. Miura, ‘‘Adsorption and Growth Inhibition of Bacteria on Carbon Materials Containing Zinc Oxide,’’ Carbon, 39, (2001) 1643-1651.

[17] Y. Kikuchi, Q. Qian, M. Machida, H. Tatsumoto, ‘‘Effect of ZnO Loading to Activated Carbon on Pb(II) Adsorption from Aqueous Solution,’’ Carbon, 44, (2006)195-202.
[18] S. Ahmed, M.G. Rasul, R. Brown, M.A. Hashib, Influence of parameters on the heterogeneous photocatalytic degradation of pesticides and phenolic contaminants in wastewater: A short review, J. Environ. Manage. 92 (2011) 311–330.
[19] B.D. Cullity, Elements of X–ray Diffraction (Reading, MA, Addison-esley, (1978), p. 102
[20] K.Y.Foo, B.H. Hameed, Preparation of oil palm (Elaeis) empty fruit bunch activated carbon by microwave-assisted KOH activation for the adsorption of methylene blue, Desalination 275 (2011) 302-305.
[21] Y. Guo, D. A. Rockstraw, Physical and chemical properties of carbons synthesized from xylan, cellulose, and Kraft lignin by H_3PO_4 activation, Carbon 44 (2006) 1464–1475.
[22] R. Baccar, J. Bouzid, M. Feki, A. Montiel, Preparation of activated carbon fromTunisian olive-waste cakes and its application for adsorption of heavy metal ions, J. Hazard. Mater. 162 (2009) 1522–1529.
[23] Y. Guo, D.A. Rockstraw. Physicochemical properties of carbons prepared from pecan shell by phosphoric acid activation, Bioresour Technol;98 (8): (2007)1513-1521.
[24] L. Zhang, H. Cheng, R. Zong, Y. Zhu, Photocorrosion Suppression of ZnO Nanoparticles via Hybridization with Graphite-like Carbon and Enhanced Photocatalytic Activity, J. Phys. Chem. C (2009), 113, 2368–2374.
[25] N. Vigneshwaran, S. Kumar, A.A. Kathe, P.V. Varadarajan, V. Prasad, Functional finishing of cotton fabrics using zinc oxide–soluble starch nanocomposites, Nanotechnology 17 (2006) 5087-5095.
[26] W. Zhao, Z. Bai, A. Ren, B. Guo, C. Wu, Sunlight photocatalytic activity of CdS modified TiO_2 loaded on activated carbon fibers Appl. Surf. Sci. 256 (2010) 3493–3498.
[27] K. Vanheusden, W.L. Warren, C.H. Seager, D.R.Tallant, J.A. Voigt, Mechanisms behind green photoluminescence in ZnO phosphor powders, J. Appl. Phys. 79, (1996)7983-7990.
[28] M. Ahmad, E. Ahmed, Z.L. Hong, N.R. Khalid, W. Ahmed, A. Elhissi, Graphene–Ag/ZnO nanocomposites as high performance photocatalysts under visible light irradiation, Journal of Alloys and Compounds 577 (2013) 717–727.
[29] A.B. Djurisic, Y.H. Leung, C.W. C. H. Choy, K.W. Cheah,; W.K.Chan, , Visible photoluminescence in ZnO tetrapod and multipod structures, Appl. Phys. Lett. 84, (2004) 2635-2637.
[30] N. Sapawe, A.A. Jalil, S. Triwahyono, S.H. Adam, N.F. Jaafar, M.A.H. Satar, Isomorphous substitution of Zr in the framework of aluminosilicate HY by an electrochemical method: Evaluation by methylene blue decolorization, Appl.Catal., B: Environ. 125 (2012) 311–323
[31] S. Lagergren, About the theory so-called adsorption of soluble substances, Kung. Sven. Veten. Hand. 24 (1898) 1–39.
[32] Z.A. AL-Othman, R. Ali, M. Naushad, Hexavalent chromium removal from aqueous medium by activated carbon prepared from peanut shell: adsorption kinetics, equilibrium and thermodynamic studies, Chem. Eng. J. 184 (2012) 238-247.
[33] B. Singha, S.K. Das, Adsorptive removal of Cu(II) from aqueous solution and industrial effluent using natural/agricultural wastes, Colloids Surf. B 107 (2013) 97–106.

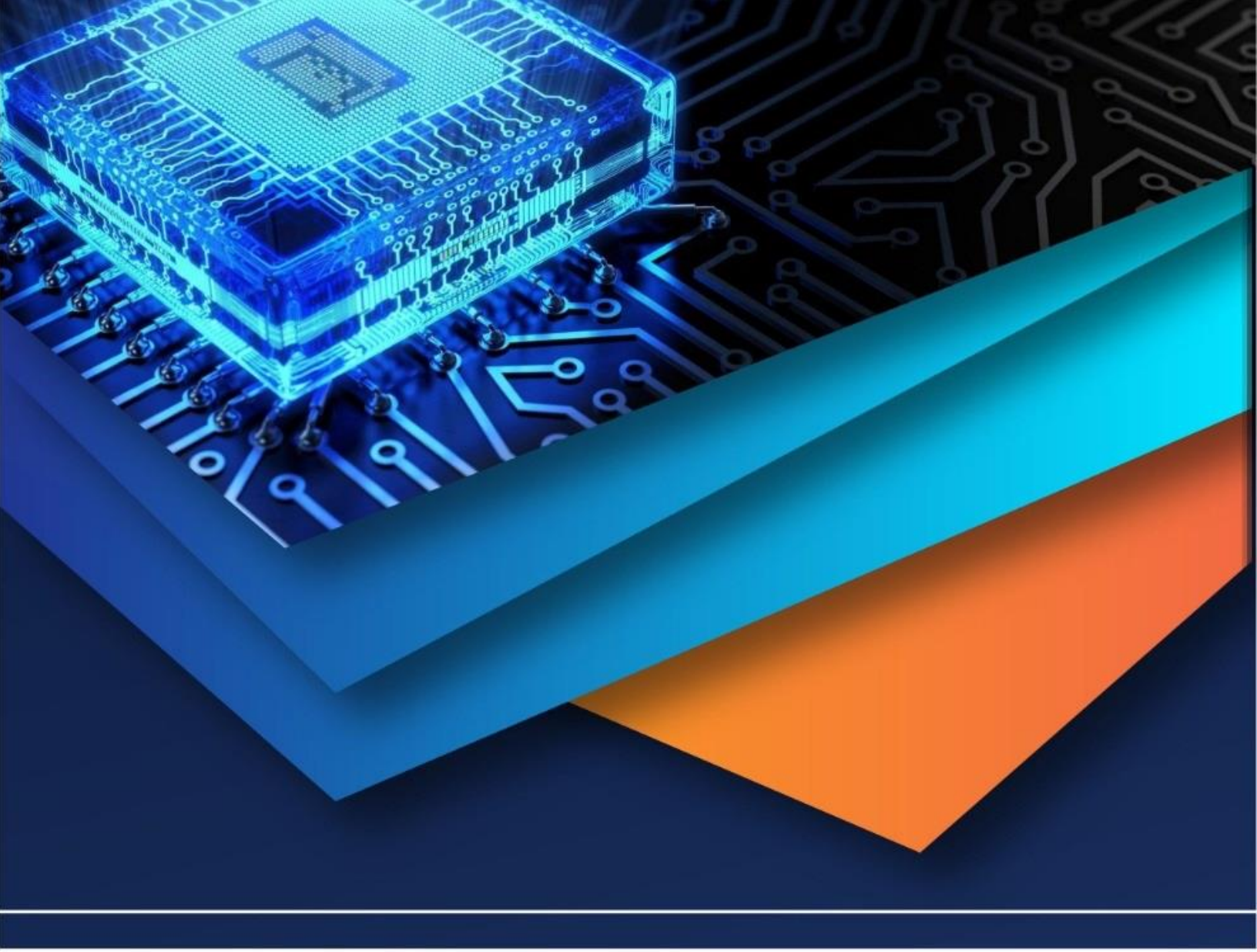

10.22214/IJRASET

45.98

IMPACT FACTOR: 7.129

IMPACT FACTOR: 7.429

INTERNATIONAL JOURNAL FOR RESEARCH

IN APPLIED SCIENCE & ENGINEERING TECHNOLOGY